Bioelectrochemistry 140 (2021) 107815

Contents lists available at ScienceDirect

Bioelectrochemistry

journal homepage: www.elsevier.com/locate/bioelechem

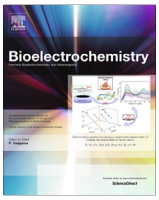

Quantitative determination of creatinine from serum of prostate cancer patients by *N*-doped porous carbon antimony (Sb/NPC) nanoparticles

Maryam Jamil [a], Batool Fatima [a,*], Dilshad Hussain [b], Tahir Ali Chohan [c], Saadat Majeed [d], Muhammad Imran [e], Ashar Ahmad Khan [f], Sumaira Manzoor [d], Rahat Nawaz [d], Muhammad Naeem Ashiq [d], Muhammad Najam-ul-Haq [d,*]

[a] Department of Biochemistry, Bahauddin Zakariya University, Multan 60800, Pakistan
[b] International Center for Chemical and Biological Sciences, HEJ Research Institute of Chemistry, University of Karachi, Karachi 75270, Pakistan
[c] Institute of Pharmaceutical Sciences, University of Veterinary and Animal Sciences, Lahore, Pakistan
[d] Institute of Chemical Sciences, Bahauddin Zakariya University, Multan 60800, Pakistan
[e] Biochemistry Section, Institute of Chemical Sciences, University of Peshawar, 25120, Pakistan
[f] Department of General Surgery, Nishtar Medical University Multan, Pakistan

ARTICLE INFO

Article history:
Received 5 January 2021
Received in revised form 26 March 2021
Accepted 30 March 2021
Available online 05 April 2021

Keywords:
Sb/NPC
Creatinine
Prostate cancer
Electrochemical sensing
Serum samples

ABSTRACT

Creatinine is an indicator of hindrance in urination and renal insufficiency. Creatinine levels are the marker of the late stages of prostate cancer. Early and sensitive detection of creatinine can reduce deaths associated with prostate cancer. In this work, nitrogen-doped porous carbon antimony (Sb/NPC) nanoparticles are fabricated to be employed as a non-enzymatic biosensor. Sb/NPC has promising redox activity and is synthesized by a two-step reaction using low-cost precursors. Electrochemical sensing by Sb/NPC is conducted for standard creatinine solutions on a three-electrodes system. Cyclic voltammetry, amperometry, and electrochemical impedance spectroscopy are used to sense creatinine. LOD and LOQ of the Sb/NPC modified electrode are 0.74 μM and 2.4 μM, respectively. This electrode system analyzes creatinine in the serum of prostate cancer patients who have elevated PSA levels. More than 90% creatinine is recovered from a spiked serum sample of a prostate cancer patient. A direct relation is observed between PSA levels and creatinine levels in prostate cancer. The developed cyclic voltammetric setup detects trace concentrations of creatinine in serum.

1. Introduction

Cancer has been playing havoc by causing 7.6 million deaths throughout the world [1]. The death rates are on the rise and reasons are not clearly understood. Some of the factors may include aging and increasing population [2]. Cancer is generally combated through chemotherapy, surgical removal of tumors, and radiotherapy. These therapeutics become less efficient because of drug resistance, drug metabolic rates, and lesser drug selectivity for tumor cells [3]. Prostate cancer is the third leading cancer [4] and originates from the outer coat of the prostate where it undergoes epigenetic variations. Serum creatinine levels are the biomarker of prostate cancer and their fluctuations can prognosis prostate cancer [5]. Diagnostics of prostate cancer is better made by estimating the PSA levels [6], however, no method measures PSA specifically and sensitively. Besides PSA, other parameters are looked at in several prostate cancer patients that have shown normal PSA levels [7]. A relation between metastatic prostate cancer or tumor stage and sarcosine/creatinine ratio also serves as a clinical indicator [8]. Creatinine can also be a marker for the late stages of prostate carcinoma [9,10].

Other than the Jaffe method, creatinine is determined spectrophotometrically [11]. GC-MS is also integrated with the Jaffe method for finding creatinine in urine [12]. HPLC is used for determining creatinine in the serum of mice [13]. Electrophoretic methods detect creatinine from urine [14]. These strategies for creatinine detection have limitations such as the number of sample preparation steps, slower detection, difficult apparatus handling, and higher limits of detection.

Nanomaterials as biosensors are advantageous due to precise results [15–17]. Nanomaterials are also used as fluorescent [18], chemiluminescent [19], and immunosensors [20,21] for the detection and recognition of biomolecules [22]. Nanoparticles coated on

* Corresponding authors.
E-mail addresses: batoolfatima@bzu.edu.pk (B. Fatima), najamulhaq@bzu.edu.pk (M. Najam-ul-Haq).

https://doi.org/10.1016/j.bioelechem.2021.107815
1567-5394/

electrodes have enhanced surface area for binding of species and thus better sensing [23–25]. Electrochemical nano-bio sensors developed for creatinine detection are the platinum electrode modified with zinc oxide-chitosan-c-MWCNT/polyaniline [26], iron oxide/chitosan graft polyaniline composite film [27], carbon nanofibers coated with polymeric dye-based metal [28], and Cu doped dendritic poly methylene blue (PMB) [28]. Quantum dots of cadmium selenide are also used for the analysis of creatinine in urine [29]. Nickel nanocomposites are assembled on a glassy carbon electrode (GCE) and CuO-MIP/CPE is immobilized on a carbon electrode for creatinine detection [30,31]. Fe_3O_4 over polyaniline nanoparticles (Fe_3O_4@PANI NPs) based molecularly imprinted electrochemical sensor (MIES) is also used for creatinine detection [4]. Ag coated ZnO/Fe_3O_4 composite for SERS photochemically detects creatinine from urine [32]. CuNPs/PDA-rGO-NB/GCE coupled ratiometric electrochemical biosensing senses creatinine [33]. Nickel nanoclusters (NiNCs) over molecularly imprinted polymers (MIPs) detect creatinine via electrochemiluminescence detector [34]. PEI-CdS/Au@SiO_2@RuDS/PANI and creatinine imprinted poly film detect creatinine using the same approach [35].

In this work, Sb/NPC is synthesized in a two-steps reaction. Sb/NPC is selected due to its high conductivity and promising redox activity and easy synthesis. Moreover, its rod-like structure provides more surface active sites. It is synthesized from low-cost precursors, which is another advantage of the study. The electrode is modified by coating with Sb/NPC nanomaterial for non-enzymatic sensing of creatinine first in PBS buffer under the optimized conditions and then from serum samples of prostate cancer patients.

2. Experimental

2.1. Chemical and reagents

Nickel chloride hexahydrate (99.5%), nitrilotriacetic acid (99.9%), isopropanol (99.9%), ethyl alcohol (99.9%), antimony chloride (99.9%), ethylene glycol (99.9%), streptavidin-coated microparticles, and creatinine (99.9%) were purchased from Sigma Aldrich. anti-PSA-Ab ~ biotin (Cat: MA1-10447) was obtained from Thermo Fischer Scientific. Deionized water was obtained from the Milli-Q water purification system (Merck, Millipore).

2.2. Synthesis of N-doped porous carbon antimony nanoparticles

Sb nanoparticles were synthesized by two steps methodology, as reported earlier [36]. In the first step, nickel chloride (1.4 g) was dissolved in a mixture of deionized water (30 mL) and isopropanol (10 mL). 0.6 g of nitrilotriacetic acid (NTA) was added and the suspension was stirred for 30 min. The mixture was transferred to a Teflon-lined autoclave and reacted for 6 h at 180 °C. After cooling, the product was washed with isopropanol and ethyl alcohol thrice, respectively. Obtained Ni/NTA precursors were dried overnight in an oven at 60 °C. The dried product was annealed in an argon furnace at 600 °C and Ni/NPC was obtained.

In the second step, Ni/NPC and $SbCl_3$ were reacted by *in situ* replacement reaction of Ni with Sb. Ni/NPC (70 mg) and $SbCl_3$ (700 mg) were sonicated at 35 °C for a half-hour in the presence of ethylene glycol (40 mL). The mixture was sealed in a Teflon-lined autoclave and heated overnight in an oven at 150 °C. The obtained Sb/NPC nanoparticles were filtered, washed, and dried in an oven for 12 h at 60 °C.

2.3. Electrochemical sensing of creatinine by Sb/NPC-GCE

Different concentrations of creatinine in PBS were electrochemically sensed on a three-electrodes system of cyclic voltammetry. The electrodes were washed in ethanol and water via sonication. Sb/NPC nanoparticles were deposited on a glassy carbon electrode through the homogenous slurry and dried at room temperature. Sb/NPC-GCE was used as a working electrode, platinum wire as a counter electrode, and Ag/AgCl as a reference electrode. Creatinine solutions of different concentrations were prepared in PBS. All the measurements were taken at room temperature. Experimental parameters like concentration, pH, interferences, the limit of detection, the limit of quantification, recovery, and stability were optimized.

2.4. Serum sample collection and Elecsys total PSA assay

Serum samples from the prostate cancer patients were collected from Nishtar Medical University Multan after prior approval and under the guidelines of the Ethical Committee.

Elecsys® total PSA quantitatively determines prostate-specific antigen (PSA). Total PSA includes PSA either coupled or free found in serum and plasma. This assay is paired with a digital rectal examination (DRE) for diagnosing prostate cancer patients. It is an electrochemiluminescence immunoassay "ECLIA" used on Elecsys and Cobas E Immunoassay Analyzers.

The sandwich principle was followed for PSA detection. The test duration was 18 min. In the first incubation, a 20 μL sample was reacted with biotinylated monoclonal PSA-specific antibody and a monoclonal Prostate-specific antibody labeled with ruthenium, causing complexation. In the second incubation, streptavidin-coated microparticles were added to the above-formed complex. This incubation caused the binding of the solid phase via the interaction of biotin and streptavidin. The reaction mixture was then aspirated into the measuring cell where microparticles under the influence of magnetic field got trapped onto the electrode. The unattached particles were washed away and ProCell/ ProCell M. Chemiluminescent emission was produced at the applied potential. Illuminant emission was determined by a photomultiplier. The calibration curve was obtained by 2-point calibration and a master curve was used for determining PSA levels.

3. Results and discussion

3.1. Morphological characterization of Sb/NPC

Sb/NPC are synthesized by *in situ* nanoconfined replacement reaction [36]. In the first step, Ni-NTA nanowire precursors are fabricated by hydrothermal reaction (Equation (1)).

$$Ni^{2+} + 2H_3NTA + 2H_2O = H_4Ni(NTA)_2{\cdot}2H_2O + 2H^+ \quad (1)$$

The precursor is annealed in argon at 650 °C for 2 h resulting in the pyrolysis of NTA into *N*-doped porous carbon (NPC). Nickel ions in the precursor are reduced to Ni nanoparticles and adsorbed onto porous carbon (Ni/NPC). In the last step, Ni is replaced by Sb nanoparticles via *in situ* nanoconfined replacement and one dimensional Sb/NPC are formed.

An aqueous solution of Sb/NPC particles is prepared for UV analysis and nickel appears at 204 nm which is the characteristic surface Plasmon resonance (SPR) of metallic nickel (Fig. S1A). Antimony is observed at 216 nm as reported earlier [37]. A broad peak at 281 nm depicts carbon matrix in the sample regarding π-π* of C and C double bond and shifting of n-π* C═C/C═, respectively. FTIR spectra of Sb and Ni/NPC are taken on JASCO FTIR 4200 spectrometer (Fig S1B). IR spectrum of Ni/NPC shows peaks at 1444, 1576, and 1645 cm^{-1} referring to C═N and nickel as a result of annealing at 650 °C. A peak at 1050 cm^{-1} suggests the presence of Sb/N which confirms the substitution between Sb and C═N.

X-ray diffraction (XRD) of Sb/NPC is carried out on Advanced Bruker D8 Discover X-ray diffractometer having non-monochromatic Cu Kα X-ray radix at 2θ ranges scanned at 20°–100°. X-ray transparent beryllium inlet is used for the placement of electrodes. The peaks of diffraction angle are indexed to standard diffraction data of metallic Sb (jcpd card 350732). The lattice structure of composites shows peaks at 22, 30, 41, 45, 48, 55, 67, 81, 86, and 96 which are assigned as (003), (101), (012), (104), (015), (202), (122), (214), (125) and (1010) showing crystal planes of the hexagonal rhombohedral structure of Sb (Fig S1C). The highest intensity peak is at 46° correspondings to (015) diffraction mode. Peaks at 35° and 42° depict the presence of N doped porous carbon. The refined lattice parameters in hexagonal (rhombohedral) Sb pure crystal parameter phases are a = b = 4.309 Å and c = 11.288 Å. Scherer equation is applied for the size confirmation of crystals (Equation (2)).

$$D = 0.9.\lambda/\beta.\mathrm{Cos}\theta \quad (2)$$

λ = X-ray wavelength used, β = Peak value at the half peak height, and θ = Angle of incidence. The size of Sb nanoparticles is 16 nm by applying this equation.

TGA (thermogravimetric analysis) is carried out for the compositional evaluation of Sb/NPC (Fig. S1D). It confirms carbon as well as antimony content in Sb/NPC. Initially, the weight loss is observed at 100 °C and it continues till 600 °C. From 100 to 450 °C, the little weight loss is due to the loss of adsorbed water leaving behind *N*-doped porous carbon antimony nanoparticles. Major weight loss occurs from 450 °C to 600 °C that is due to the decomposition of organic precursors. Sb content in the composite is calculated as 67.9%.

The structure and morphology of Ni/NPC and Sb/NPC are shown in SEM images (Fig. 1A and 1D). The diameter of Ni/NPC is 55 nm and that of Sb/NPC is 14 nm. Sb/NPC particles are evenly distributed in nitrogen-carbon porous web structure (Fig. 1B and 1E). AFM analysis shows the surface topology of nanoparticles of Ni and Sb/NPC (Fig. 1C and 1F).

3.2. Electrochemical characterization of Sb/NPC-GCE

3.2.1. Electrochemical surface area

For determining the electrochemical surface area (ECSA) of Sb-NPC/GCE, the conductivity of the modified electrode system is estimated using the solutions of $K_3[Fe(CN)_6]$ and potassium chloride (Fig. S2). Cyclic voltammetric results of Sb-NPC/GCE immersed in the given solution are different from bare GCE. For further calculations, the active surface area of the electrode system involved in the electrochemical phenomenon is calculated at different scan rates in the range of 20–70 mVs^{-1}. Randles-Sevcik equation is applied as given in Eq. (3) [38].

$$\text{Peak current} = \pm \left(2.69 .10^5\right) \text{n X } 3/2.\ \text{A XD}/2\ \text{CX v}/2 \quad (3)$$

where A = Area of an electrode surface (cm^2), D = Diffusion coefficient = 7.2 × $(10)^{-6}$ cm^2 s^{-1}, n = Numbers of electrons in oxidation-reduction reaction = 1, C = Concentration of $K_3[Fe(CN)_6]$ = 0.04 mM. The electrochemical surface area for bare GCE, A is 0.073 cm^2 and for Sb/NPC is 0.144 cm^2.

3.2.2. Roughness factor

The roughness factor of Sb/NPC-GCE and bare GCE is measured by calculating the peak current, I_P, and from the peak current, the electrochemical surface area is calculated. The roughness factor depends on the number of redox cycles occurring on the dimensions of the electrode surface area [39]. The roughness factor (fr) of electrodes is calculated by Eq. (4).

$$\text{Roughness factor}\,(fr) = A_2/A_1 \quad (4)$$

where A_2 is the electrochemical surface area of bare Sb/NPC and A_1 is the electrochemical surface area of bare GCE. So, the roughness factor can be derived by the ratio of the surface area of the bare electrode and Sb/NPC-GCE and the value is 1.97. This value indicates the higher charge transfer in the case of Sb/NPC-GCE due to more roughness of the electrode surface after deposition of material.

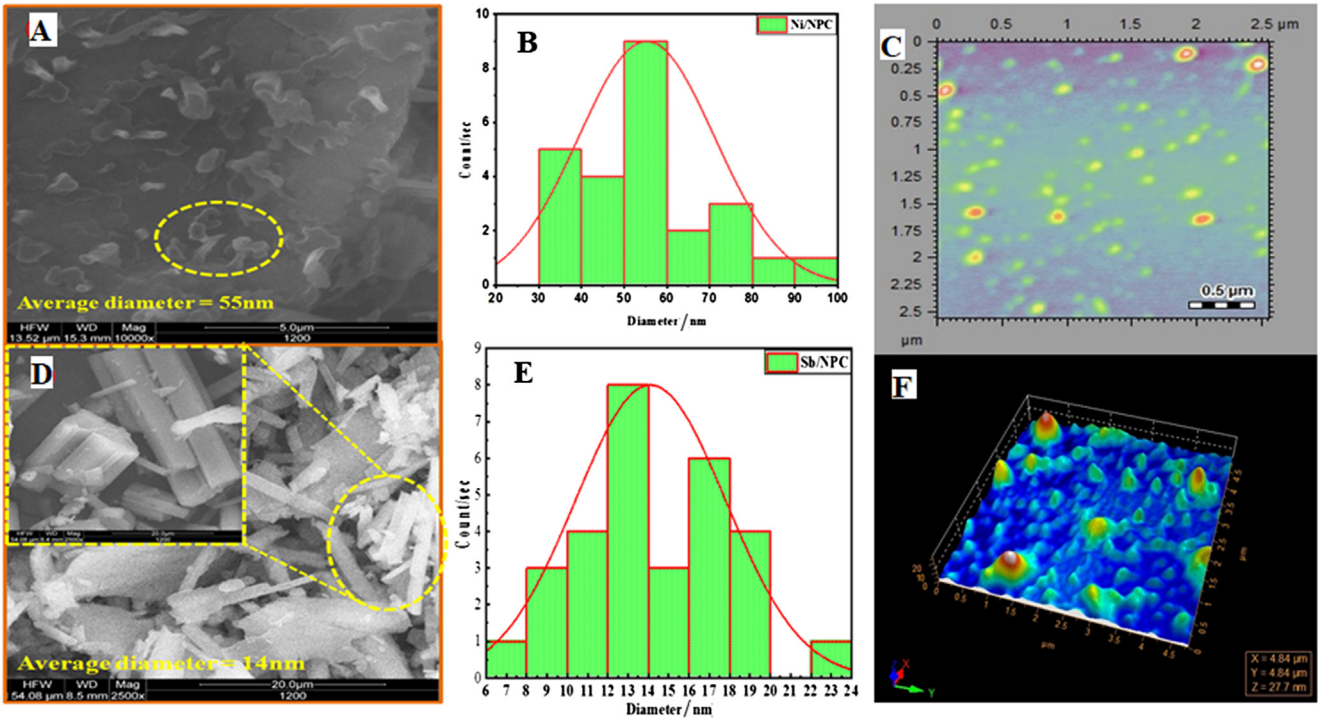

Fig. 1. (A) SEM, (B) Particle size distribution, and (C) AFM of Ni/NPC, and (D) SEM, (E) Particle size distribution, and (F) AFM of Sb/NPC.

3.3. Electrochemical parameters optimization of Sb/NPC by cyclic voltammetry

Redox activities of Ni/NPC and Sb/NPC modified electrodes are measured in $K_3[Fe(CN_6)]$ solution by cyclic voltammetry. For comparison, a blank electrode is also run. The voltage window is set on 0.8–0.5 V and the scan rate as 30 mVs^{-1} (Fig. S3). Blank electrode shows some oxidation-reduction potentials due to the presence of iron radical in potassium ferrocyanide. The redox potential of Ni/NPC is more than that of blank due to the conductive nature of Nickel. The highest conductivity is observed for Sb/NPC because of elevated oxidation-reduction potential.

To optimize the electrochemical parameters, different concentrations of creatinine solutions (0.6–1.0 μM) were analyzed by cyclic voltammetry. The potential window is set at −0.2–0.10 V and the scan rate is kept at 30 mVs^{-1}. Anodic peaks current increases with the increase in concentration (Fig. 2A). The reduction peak current of the cathode decreases with an increase in concentration. The highest oxidation peak is obtained at 0.6–0.8 V and reduction at 0.4 V. A linear relationship is attained between the concentration of creatinine and current (Fig. 2D).

Limit of detection (LOD) and limit of quantification (LOQ) for Sb/NPC-GCE are calculated by following Eqs. (5) and (6).

$$LOD = 3S/m \quad (5)$$

$$LOQ = 10.S/m \quad (6)$$

where S is the standard deviation = 3.07×10^{-7}, m is the slope = 1.24×10^{-6}. LOD and LOQ for Sb/NPC-GCE are 0.74 μM and 2.4 μM, respectively.

The effect of scan rate for sensing creatinine by Sb/NPC-GCE is also studied. By increasing the scan rates from 20 to 70 mVs^{-1}, the current also increases. The highest peak is measured at 70 mVs^{-1}. A direct relation between scan rate and oxidation-reduction peak is thus observed (Fig. 2B and 2E). The pH of the buffer also influences the detecting capability of material as pH alters linkage between template molecules and the sensing material of electrode [40]. The impact of buffer pH is evaluated at a pH range of 7.2 to 8.0. The creatinine peak current increases from 7.2 to 7.6. Maximum peak current is obtained at physiological pH i.e 7.4. After 7.6, no prominent increase in peak current is observed (Fig. 2C and 2F). At pH below physiological pH, lesser electrostatic interactions occur that generate small signals. As pH increases from 7.4, lesser protonation of creatinine amino acids leads to lesser signals. So, the PBS buffer of pH 7.4 maximizes the sensitivity of the creatinine sensor. Anodic peak goes toward less positive values with increasing pH. Oxidation of creatinine gives one electron and one proton per molecule of creatinine [28]. So, creatinine can be electrochemically detected by measuring its oxidation current. The cyclic voltammetric detection of creatinine over the Sb/NPC coated sensor is due to the fine electrocatalytic and conductive activity of Sb/NPC-GCE.

3.4. Electrochemical impedance analysis

There are a variety of factors that influence the impedance of the electrode system. Initially, the effect of modification of electrode on impedance is studied. Greater the conductivity of a material, lesser is the impedance as is observed for Ni/NPC, Sb/NPC, and bare GCE. Sb/NPC is the most conductive and shows the least impedance while bare GCE is the least conductive and shows maximum impedance. Ni/NPC exhibits intermediate behavior for impedance (Fig. 3A). The impedance at different concentrations is also studied. The least impedance is observed at 0.8 mM concentration that indicates the least resistance (Fig. 3B). Above or below this concentration, a rise in impedance is recorded. Slight complex behavior is observed at different concentrations, this may be due to fouling of electrode surface during the electrochemical reaction [41]. Oxidation of creatinine can change the charge transfer process due to the formation of oxidized products (Scheme 1). Altering the pH of the buffer system also affects impedance. Buffer pH for Sb/NPC modified electrode system is varied as 7.0, 7.2, 7.4, 7.6, 7.8 and

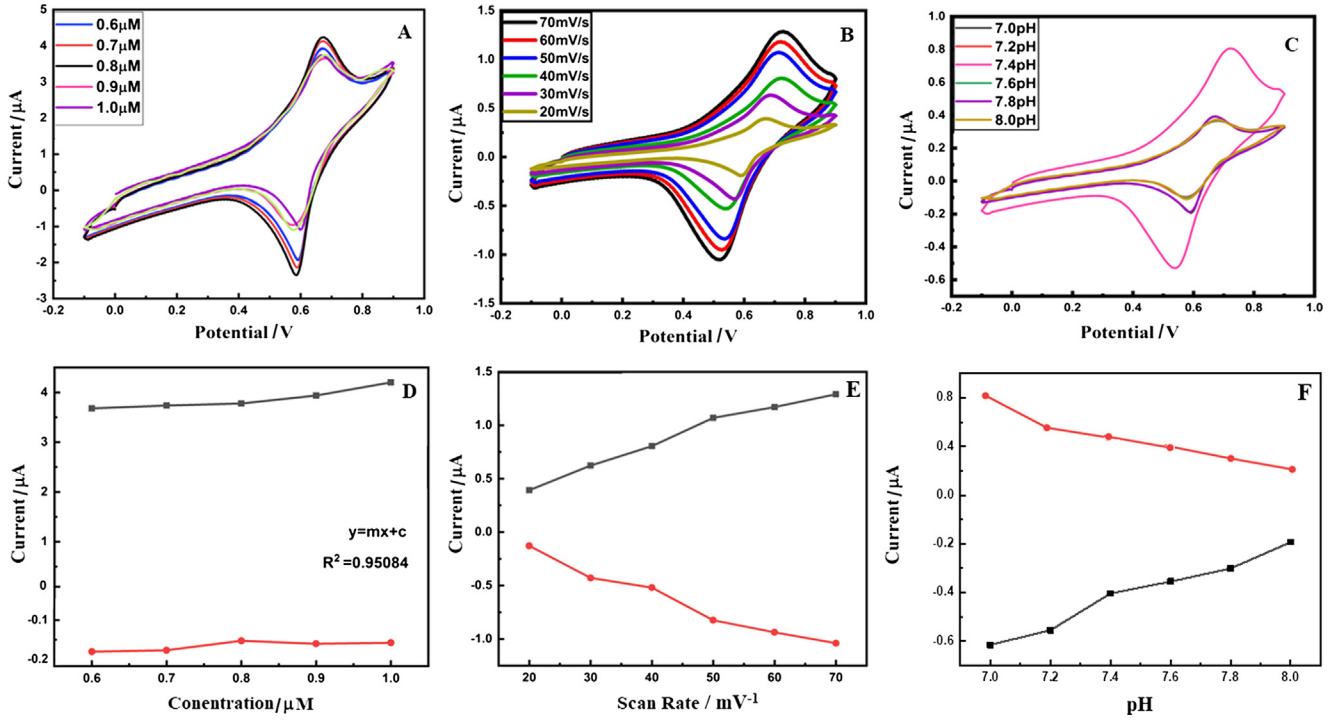

Fig. 2. Cyclic voltammogram of (A) Different concentrations of creatinine 0.6–1.0 μM in 0.1 M PBS of pH 7.4, (B) Scan rates in the range of 20 to 70 mVs^{-1}, and (C) Effect of pH on Sb/NPC-GCE. Corresponding calibration curves of (D, E, and F) concentrations, scan rates, and pH. (—■—: oxidation, —●—: reduction).

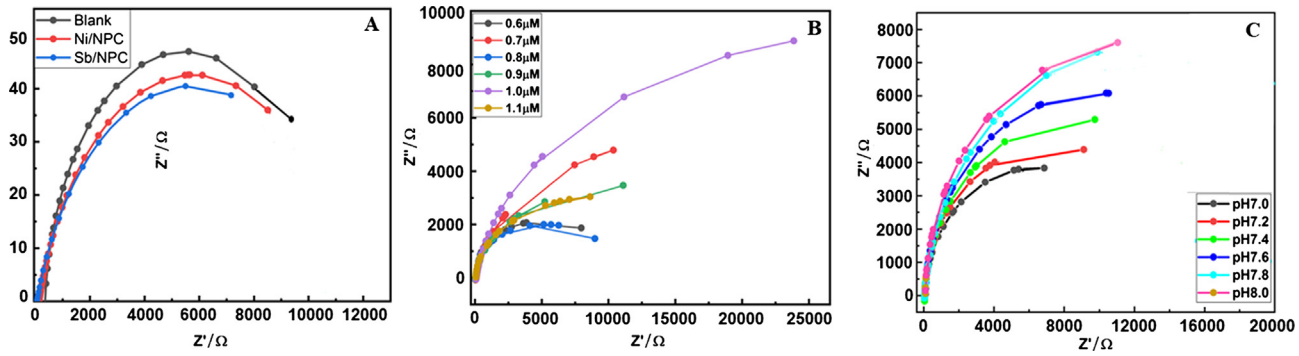

Fig. 3. (A) Impedance of Ni, Sb/NPC, and blank electrode, (B) Impedance and concentration relationship, and (C) pH effect on impedance.

8.0. The electron transfer resistance increases with the increase in pH. A direct relation between impedance and pH is shown in Fig. 3C. Rct value for bare GCE is 1290 Ω and for Sb/NPC is 1131 Ω. Rct values for concentration and pH are presented in Table S1 (supporting information). A lower Rct value for Sb/NPC-GCE than bare GCE indicates lower charge transfer resistance.

3.4.1. Heterogeneous rate constant (K°)

The standard heterogeneous rate constant (K°) can be drawn by using EIS to modify each electrode. K° gives the kinetics of the redox reaction. A system having a greater value of K° would achieve equilibrium more rapidly and sustain its equilibrium for a greater period as compared to that of a low K° value system. K° values are calculated by Equation (7);

$$K^{\circ} = RT/(F)^2 R_{ct}.A.C \quad (7)$$

where R = Global gas constant = 8.314 J mol^{-1} K^{-1}, T = Thermodynamic temperature = 298.15 K, F = Constant for Faraday = 96,485C mol^{-1}, R_{ct} = Electron transfer resistance = 1131 Ω (Sb), 1290 (GCE), A = Electrode surface area = 0.73 cm^2, and C = Concentration of $K_3[Fe(CN)_6]$ = 0.04 mM.

K° for bare GCE and Sb/NPC-GCE are 7.07×10^{-8} cms^{-1} and 1.76×10^{6} cms^{-1} respectively. K° value of Sb-NPC/GCE (8.06×10^{-8} cms^{-1}) is greater than bare GCE (7.07×10^{-8} cms^{-1}) that depicts the stability and equilibrium maintenance capability of Sb-NPC/GCE system in electrochemical biosensing [42]. Hence, Sb/NPC electrochemical sensor offers a swift transfer of electrons than that of the bare electrode [43].

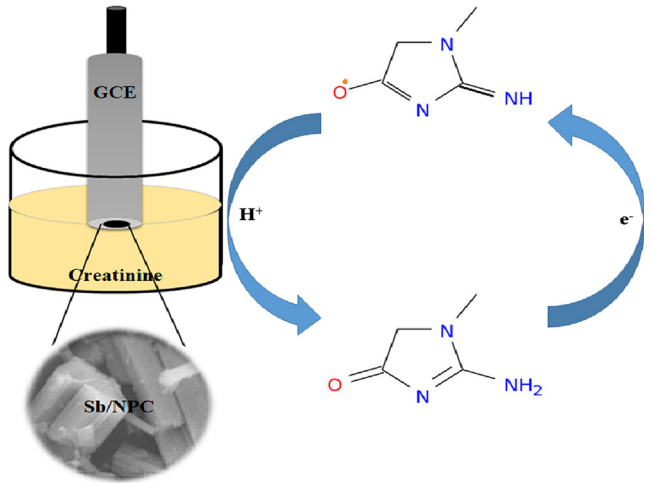

Scheme 1. Mechanism of electrochemical sensing of creatinine by Sb/NPC-GCE.

3.5. Effect of interfering substances

Non-specific interfering species are encountered when biological molecules are electrochemically analyzed. Interfering species are added to creatinine solution in 0.1 M PBS to observe the effect (Fig. S4). Urea, uric acid, glycine, lactose, sarcosine, glucose, and ascorbic acid are added at their physiological concentrations. None of the contaminants gives a distinct peak. Urea appears at a higher potential that leads to a slight decrease in current for creatinine detection. Sb/NPC deposited glassy carbon electrode is thus selective in detecting creatinine in the presence of biological interfering species.

Similarly, the effect of NH_2 containing biomolecules on creatinine sensing is evaluated and results are presented in Fig. S5. CV of the mixture containing, urea, uric acid, lysine, and creatinine is taken oven Sb/NPC in PBS buffer of biological pH to check the interfering effect. It is observed that these molecules did not affect the detection of creatinine. However current produced by the creatinine is reduced due to the presence of these molecules.

3.6. Stability and reproducibility of Sb/NPC modified electrode

The electrode is set at 30 redox cycles for verifying the stability of the Sb/NPC modified electrode by cyclic voltammetry. A specific continuous pattern of redox peaks is obtained where oxidation peak is at 0.4 V and reduction at 1.0 V (Fig. 4A). The stability of the Sb/NPC modified electrode is also evaluated by chronoamperometry (Fig. 4B). A linear response is recorded for creatinine at the scan rate of 30 mV/s. Current decreases for 1000 s and becomes stable for more than 4000 s. The steady-state current suggests the electrode system as a steady-state energy source.

3.7. Recovery analysis of creatinine by Sb/NPC-GCE from serum sample

Sb/NPC-GCE analyzes creatinine from serum samples via recovery testing. The serum samples are spiked with known creatinine concentration. The calculated recoveries from five serum samples are in the range of 94% to 100% (Table S2). Mechanism of sensing of creatinine is given in scheme 1. Electrostatic interactions and π-π stacking are the main forces between aromatic creatinine and Sb/NPC. Sb particles offer electrostatic interactions, while π-π of porous carbon facilitates the charge transfer between the electrode surface and the electrolyte.

3.8. Quantitative determination of creatinine from serum samples of prostate cancer

The serum creatinine and PSA levels are associated with a high risk of prostate cancer [5] as can be seen by the obtained data here. Normal ranges of creatinine in blood may be from 0.84 to 1.21 mg

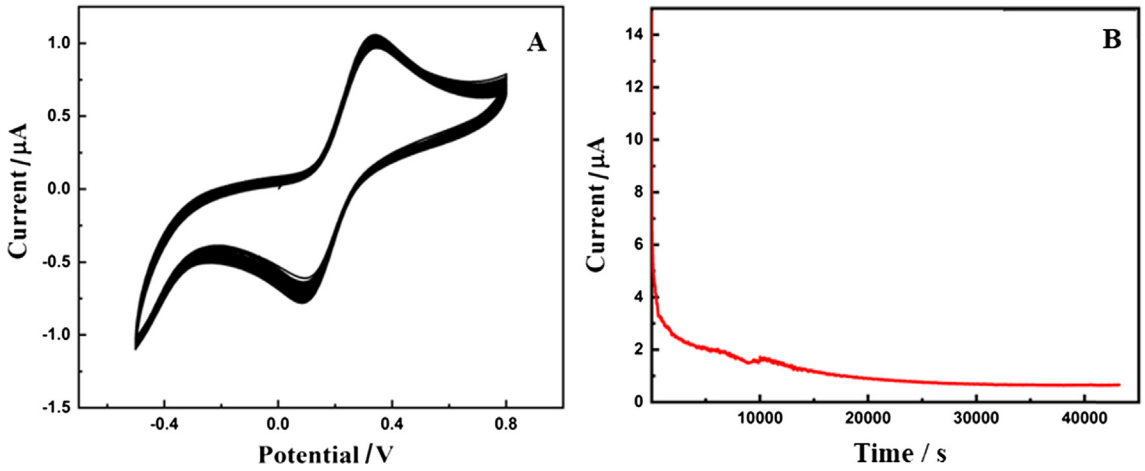

Fig. 4. Stability and reproducibility of Sb/NPC-GCE by, (A) Cyclic voltammetry for 30 cycles in 0.1 M potassium phosphate buffer of pH 7.4, and by (B) Chronoamperometry up to 40000s.

Table 1
Comparison of PSA level (determined by Elecsys total PSA analysis) and creatinine concentration (obtained from electrochemical sensing) in prostate cancer patient serum.

Sample No.	PSA value (ng mL^{-1})	Current (A)	Conc. of Creatinine (mg dL^{-1})	Scan rate (Vs^{-1})	Potential window (V)
1	04	-4.3710^{-7}	0.99	0.03	−0.5 to 0.8
2	25	-1.18×10^{-7}	1.75	0.03	−0.5 to 0.8
3	99	-1.04×10^{-7}	2.56	0.03	−0.5 to 0.8
4	525	-1.01×10^{-7}	3.71	0.03	−0.5 to 0.8
5	978	-3.3×10^{-6}	5.15	0.03	−0.5 to 0.8
6	1057	-2.1×10^{-6}	5.59	0.03	−0.5 to 0.8
7	1130	-2.1×10^{-6}	6.03	0.03	−0.5 to 0.8
8	1133	-1.9×10^{-6}	6.15	0.03	−0.5 to 0.8
9	1370	-1.7×10^{-6}	7.16	0.03	−0.5 to 0.8
10	1677	-1.2×10^{-6}	7.43	0.03	−0.5 to 0.8

Table 2
Comparison of different materials for electrochemical sensing with Sb/NPC nanoparticles.

Sensing Material	Target	LOD	Linear Range	Ref.
Poly ethylene-*co*-vinyl alcohol(EVAL)	Creatinine	40 ng mL^{-1}	0.05 μg mL^{-1} to 2 μg mL^{-1}	[44]
PANi-Nafion-Cu composite	Creatinine and urea	0.5 μM	1 to 125 μM	[45]
Quartz conductive sheets	Urine creatinine	–	1 to 30 mM	[46]
Fe_3O_4@ Polyaniline nanoparticles (Fe_3O_4@PANI NPs)	Urine and plasma creatinine	0.35 nmol/L		[47]
screen-printed electrode made of carbon black	Urine creatinine	0.043 mM L^{-1}	0.10–6.5 mM	[48]
platinum electrodes	Urine creatinine	4.5 M	0–500 M	[49]
Reduced graphene pasted screen printed carbon electrode	Creatinine	0.22 mM	0.01 to 2.0 mM	[28]
TGA capped Zn S: Mn -ZnS QDs	Creatinine	7.25 nM	0.07 to 3.4 μM	[50]
Ni-PANI NPs	Creatinine	0.2 nM	40 to 800μM nM	[30]
PMB-PVAc-Cu-CNF/ACF	Creatinine	0.2 ng mL^{-1}	0.5–900 ng	[28]
CuO nanoparticles -MIP/CPE electrode	Creatinine	0.083 M	0.5 to 200 M	[31]

dL^{-1}. The samples are first analyzed by Elecsys Assay to evaluate the PSA levels where samples show different PSA concentrations. Sb/NPC-GCE is then used for the quantitative determination of creatinine in prostate cancer serum samples under the optimized conditions (Fig. S6). The creatinine concentration increases in the serum samples with higher PSA levels (Table 1). A comparison of Sb/NPC-GCE with other electrochemical sensors is given in Table 2.

4. Conclusion

One-dimensional nitrogen-doped porous carbon nickel (Ni/NPC) and antimony (Sb/NPC) nanoparticles are synthesized by a two-step hydrothermal method. Nickel is displaced with antimony on NPC through *in situ* displacement method. SEM, AFM, FTIR, XRD, UV, and TGA confirm the synthesis, size, morphology, structure, and thermal stability of Sb/NPC. Sb/NPC shows better electrochemical results compared to Ni/NPC. Sb/NPC is optimized for creatinine detection at different concentrations, scan rates, and pH in PBS. The stability of Sb/NPC is estimated by cyclic voltammetry for 30 cycles at the potential window of −0.5 to 0.8 V. Stability is also verified by Chronoamperometry. Interfering substances are added to the creatinine solution for verifying the selectivity of Sb/NPC-GCE. The material shows recovery up to 100% in serum samples. Finally, the quantitative determination of creatinine from serum samples of prostate cancer patients shows that creatinine levels are directly related to PSA concentrations. Low-cost and sensitive non-enzymatic sensing of creatinine by the designed biosensing platform make it a point-of-care unit for the prognosis of prostate cancer.

Declaration of Competing Interest

The authors declare that they have no known competing financial interests or personal relationships that could have appeared to influence the work reported in this paper.

Appendix A. Supplementary material

Supplementary data to this article can be found online at https://doi.org/10.1016/j.bioelechem.2021.107815.

References

[1] F. Bray, J. Ferlay, I. Soerjomataram, R.L. Siegel, L.A. Torre, A. Jemal, Global cancer statistics 2018: GLOBOCAN estimates of incidence and mortality worldwide for 36 cancers in 185 countries, CA Cancer J. Clin. 68 (2018) 394–424.

[2] L. Zane, V. Sharma, T. Misteli, Common features of chromatin in aging and cancer: cause or coincidence?, Trends Cell Biol 24 (2014) 686–694.

[3] G. Xu, H.L. McLeod, Strategies for enzyme/prodrug cancer therapy, Clin. Cancer Res. 7 (2001) 3314–3324.

[4] S. Akturan, B. Gümüş, Ö. Özer, H. Balandız, A.K. Erenler, Death rates and causes of death in turkey between 2009 and 2016 based on tuik data, Konuralp Tıp Dergisi 11 (2019) 9–16.

[5] S.J. Weinstein, K. Mackrain, R.Z. Stolzenberg-Solomon, J. Selhub, J. Virtamo, D. Albanes, Serum creatinine and prostate cancer risk in a prospective study, Cancer Epidem. Prevent. Biomar. 18 (2009) 2643–2649.

[6] M. Logozzi, D.F. Angelini, E. Iessi, D. Mizzoni, R. Di Raimo, C. Federici, L. Lugini, G. Borsellino, A. Gentilucci, F. Pierella, Increased PSA expression on prostate cancer exosomes in in vitro condition and in cancer patients, Cancer Lett. 403 (2017) 318–329.

[7] M.R. Haythorn, R.J. Ablin, Prostate-specific antigen testing across the spectrum of prostate cancer, Biomar. Med. 5 (2011) 515–526.

[8] M. Wang, L. Zou, J. Liang, X. Wang, D. Zhang, Y. Fang, J. Zhang, F. Xiao, M. Liu, The urinary sarcosine/creatinine ratio is a potential diagnostic and prognostic marker in prostate cancer, Med. Sci. Monit. Int. Med. J. Exp. Clin. Res. 24 (2018) 3034.

[9] S. Vesalainen, P. Lipponen, M. Talja, K. Syrjänen, Biochemical parameters as prognostic factors in prostatic adenocarcinoma, Acta Oncol. 34 (1995) 53–59.

[10] D. Sandhu, P. Mayor, P. Sambrook, N. George, Outcome and prognostic factors in patients with advanced prostate cancer and obstructive uropathy, Br. J. Urol. 70 (1992) 412–416.

[11] H. Yatzidis, New method for direct determination of" true" creatinine, Clin. Chem. 20 (1974) 1131–1134.

[12] D. Tsikas, A. Wolf, A. Mitschke, F.-M. Gutzki, W. Will, M. Bader, GC–MS determination of creatinine in human biological fluids as pentafluorobenzyl derivative in clinical studies and biomonitoring: inter-laboratory comparison in urine with Jaffé, HPLC and enzymatic assays, J. Chromatogr. B 878 (2010) 2582–2592.

[13] P.S. Yuen, S.R. Dunn, T. Miyaji, H. Yasuda, K. Sharma, R.A. Star, A simplified method for HPLC determination of creatinine in mouse serum, Am. J. Physiol. Renal Physiol. 286 (2004) F1116–F1119.

[14] S. Wang, X. Li, J. Yang, X. Yang, F. Hou, Z. Chen, Rapid determination of creatinine in human urine by microchip electrophoresis with LED induced fluorescence detection, Chromatographia 75 (2012) 1287–1293.

[15] B. Fatima, D. Hussain, A. Saeed, M.S. Sajid, S. Majeed, R. Nawaz, M.N. Ashiq, M. Najam-ul-Haq, R. Mehmood, Tellurium doped zinc imidazole framework (Te@ZIF-8) for quantitative determination of hydrogen peroxide from serum of pancreatic cancer patients, Sci. Rep. 10 (2020) 21077.

[16] S. Tayyab Raza Naqvi, T. Rasheed, M. Naeem Ashiq, M. Najam ul Haq, S. Majeed, B. Fatima, R. Nawaz, D. Hussain, S. Shafi, Fabrication of iron modified screen printed carbon electrode for sensing of amino acids, Polyhedron 180 (2020) 114426.

[17] Y. Xu, P. Li, D. Cheng, C. Wu, Q. Lu, W. Yang, X. Zhu, P. Yin, M. Liu, H. Li, Y. Zhang, Group IV nanodots: synthesis, surface engineering and application in bioimaging and biotherapy, J. Mater. Chem. B 8 (2020) 10290–10308.

[18] Z. Ma, Y. Sun, J. Xie, P. Li, Q. Lu, M. Liu, P. Yin, H. Li, Y. Zhang, S. Yao, Facile preparation of MnO2 quantum dots with enhanced fluorescence via microenvironment engineering with the assistance of some reductive biomolecules, ACS Appl. Mater. Interfaces 12 (2020) 15919–15927.

[19] Y. Sun, Y. Zhang, H. Zhang, M. Liu, Y. Liu, Integrating highly efficient recognition and signal transition of g-C3N4 embellished Ti3C2 MXene hybrid nanosheets for electrogenerated chemiluminescence analysis of protein kinase activity, Anal. Chem. 92 (2020) 10668–10676.

[20] S. Zhang, N. Huang, Q. Lu, M. Liu, H. Li, Y. Zhang, S. Yao, A double signal electrochemical human immunoglobulin G immunosensor based on gold nanoparticles-polydopamine functionalized reduced graphene oxide as a sensor platform and AgNPs/carbon nanocomposite as signal probe and catalytic substrate, Biosens. Bioelectron. 77 (2016) 1078–1085.

[21] S. Zhang, R. Li, X. Liu, L. Yang, Q. Lu, M. Liu, H. Li, Y. Zhang, S. Yao, A novel multiple signal amplifying immunosensor based on the strategy of in situ-produced electroactive substance by ALP and carbon-based Ag-Au bimetallic as the catalyst and signal enhancer, Biosens. Bioelectron. 92 (2017) 457–464.

[22] B. Fatima, D. Hussain, S. Bashir, H.T. Hussain, R. Aslam, R. Nawaz, H.N. Rashid, N. Bashir, S. Majeed, M.N. Ashiq, M. Najam-ul-Haq, Catalase immobilized antimonene quantum dots used as an electrochemical biosensor for quantitative determination of H2O2 from CA-125 diagnosed ovarian cancer samples, Mater. Sci. Eng. C 117 (2020) 111296.

[23] R. Aslam, B. Fatima, D. Hussain, R. Nawaz, S. Majeed, M.N. Ashiq, T.I. Qureshi, M. Najam-Ul-Haq, Sensitive and high recovery electrochemical sensing of resorcinol by Cd–glutathione complex-modified glassy carbon electrode, Int. J. Environ. Anal. Chem. (2020) 1–11.

[24] S.T.R. Naqvi, B. Shirinfar, D. Hussain, S. Majeed, M.N. Ashiq, Y. Aslam, N. Ahmed, Electrochemical sensing of ascorbic acid, hydrogen peroxide and glucose by bimetallic (Fe, Ni)–CNTs composite modified electrode, Electroanalysis 31 (2019) 851–857.

[25] P. Li, C. Wu, Y. Xu, D. Cheng, Q. Lu, J. Gao, W. Yang, X. Zhu, M. Liu, H. Li, P. Yin, Y. Zhang, Group IV nanodots: newly emerging properties and application in biomarkers sensing, Trac Trends Anal. Chem. 131 (2020) 116007.

[26] B.O. Kasap, S.V. Marchenko, O.O. Soldatkin, S.V. Dzyadevych, B.A. Kurc, Biosensors based on nano-gold/zeolite-modified Ion selective field-effect transistors for creatinine detection, Nanoscale Res. Lett. 12 (2017) 162.

[27] C. Pundir, S. Yadav, A. Kumar, Creatinine sensors, Trac Trends Anal. Chem. 50 (2013) 42–52.

[28] I. Pandey, P.K. Bairagi, N. Verma, Electrochemically grown polymethylene blue nanofilm on copper-carbon nanofiber nanocomposite: an electrochemical sensor for creatinine, Sens. Actuators B 277 (2018) 562–570.

[29] S. Hooshmand, Z. Es'haghi, Microfabricated disposable nanosensor based on CdSe quantum dot/ionic liquid-mediated hollow fiber-pencil graphite electrode for simultaneous electrochemical quantification of uric acid and creatinine in human samples, Anal. Chim. Acta 972 (2017) 28–37.

[30] H. Rao, Z. Lu, H. Ge, X. Liu, B. Chen, P. Zou, X. Wang, H. He, X. Zeng, Y. Wang, Electrochemical creatinine sensor based on a glassy carbon electrode modified with a molecularly imprinted polymer and a Ni@ polyaniline nanocomposite, Microchim. Acta 184 (2017) 261–269.

[31] N. Nontawong, M. Amatatongchai, S. Thimoonnee, S. Laosing, P. Jarujamrus, C. Karuwan, S. Chairam, Novel amperometric flow-injection analysis of creatinine using a molecularly-imprinted polymer coated copper oxide nanoparticle-modified carbon-paste-electrode, J. Pharm. Biomed. Anal. 175 (2019) 112770.

[32] M.T. Alula, J. Yang, Photochemical decoration of magnetic composites with silver nanostructures for determination of creatinine in urine by surface-enhanced Raman spectroscopy, Talanta 130 (2014) 55–62.

[33] X. Gao, R. Gui, H. Guo, Z. Wang, Q. Liu, Creatinine-induced specific signal responses and enzymeless ratiometric electrochemical detection based on copper nanoparticles electrodeposited on reduced graphene oxide-based hybrids, Sens. Actuators B 285 (2019) 201–208.

[34] B. Babamiri, A. Salimi, R. Hallaj, M. Hasanzadeh, Nickel nanoclusters as a novel emitter for molecularly imprinted electrochemiluminescence based sensor toward nanomolar detection of creatinine, Biosens. Bioelectron. 107 (2018) 272–279.

[35] N. Cao, F. Zhao, B. Zeng, A novel self-enhanced electrochemiluminescence sensor based on PEI-CdS/Au@ SiO2@ RuDS and molecularly imprinted polymer for the highly sensitive detection of creatinine, Sens. Actuators B 306 (2020) 127591.

[36] Q. Yang, J. Zhou, G. Zhang, C. Guo, M. Li, Y. Zhu, Y. Qian, Sb nanoparticles uniformly dispersed in 1-D N-doped porous carbon as anodes for Li-ion and Na-ion batteries, J. Mater. Chem. A 5 (2017) 12144–12148.

[37] V.S. Marakatti, S.C. Peter, Nickel–antimony nanoparticles confined in SBA-15 as highly efficient catalysts for the hydrogenation of nitroarenes, New J. Chem. 40 (2016) 5448–5457.

[38] K. Ngamchuea, S. Eloul, K. Tschulik, R.G. Compton, Planar diffusion to macro disc electrodes—what electrode size is required for the Cottrell and Randles-Sevcik equations to apply quantitatively?, J Solid State Electrochem. 18 (2014) 3251–3257.

[39] P. Krzyczmonik, E. Socha, S. Skrzypek, K. Soliwoda, G. Celichowski, J. Grobelny, Honeycomb-structured porous poly (3, 4-ethylenedioxythiophene) composite layers on a gold electrode, Thin Solid Films 565 (2014) 54–61.

[40] B. Gao, Y. Li, Z. Zhang, Preparation and recognition performance of creatinine-imprinted material prepared with novel surface-imprinting technique, J. Chromatogr. B 878 (2010) 2077–2086.

[41] B.L. Hanssen, S. Siraj, D.K.Y. Wong, Recent strategies to minimise fouling in electrochemical detection systems, Rev. Anal. Chem. 35 (2016) 1–28.

[42] N. Jandaghi, S. Jahani, M.M. Foroughi, M. Kazemipour, M. Ansari, Cerium-doped flower-shaped ZnO nano-crystallites as a sensing component for simultaneous electrochemical determination of epirubicin and methotrexate, Microchim. Acta 187 (2020) 24.

[43] A.M. Santos, A. Wong, O. Fatibello-Filho, Simultaneous determination of salbutamol and propranolol in biological fluid samples using an electrochemical sensor based on functionalized-graphene, ionic liquid and silver nanoparticles, J. Electroanal. Chem. 824 (2018) 1–8.

[44] M. Conti, S. Moutereau, M. Zater, K. Lallali, A. Durrbach, P. Manivet, P. Eschwege, S. Loric, Urinary cystatin C as a specific marker of tubular dysfunction, Clin. Chem. Lab. Med. (CCLM) 44 (2006) 288–291.

[45] M. Zhybak, V. Beni, M. Vagin, E. Dempsey, A. Turner, Y. Korpan, Creatinine and urea biosensors based on a novel ammonium ion-selective copper-polyaniline nano-composite, Biosens. Bioelectron. 77 (2016) 505–511.

[46] D. Gaddes, W.B. Reeves, S. Tadigadapa, Calorimetric biosensing system for quantification of urinary creatinine, ACS Sensors 2 (2017) 796–802.

[47] X. Huang, Y. Li, J. Pan, F. Lu, Y. Chen, W. Gao, Glutathione-protected hierarchical colorimetric response of gold nanoparticles: a simple assay for creatinine rapid detection by resonance light scattering technique, Plasmonics 10 (2015) 1107–1114.
[48] E.L. Fava, T.M. do Prado, A. Garcia-Filho, T.A. Silva, F.H. Cincotto, F.C. de Moraes, R.C. Faria, O. Fatibello-Filho, Non-enzymatic electrochemical determination of creatinine using a novel screen-printed microcell, Talanta 207 (2020).
[49] D.A. Walsh, E. Dempsey, Comparison of electrochemical, electrophoretic and spectrophotometric methods for creatinine determination in biological fluids, Anal. Chim. Acta 459 (2002) 187–198.
[50] N. Tajarrod, M.K. Rofouei, M. Masteri-Farahani, R. Zadmard, A quantum dot-based fluorescence sensor for sensitive and enzymeless detection of creatinine, Anal. Methods 8 (2016) 5911–5920.